



## Monsoonal and westerly influences on interglacial calcite deposition and environmental conditions in southern Tibetan Plateau

Haibo Wang <sup>a,b,c</sup>, Carlos Pérez-Mejías <sup>c</sup>, Xianyan Wang <sup>b</sup> , Tingyong Li <sup>d</sup> , Can Yang <sup>a</sup>, Hanying Li <sup>c</sup>, Shihao Lei <sup>c</sup>, Youfeng Ning <sup>c</sup>, R. Lawrence Edwards <sup>e</sup>, Hai Cheng <sup>b,c,f,\*</sup>

<sup>a</sup> School of Engineering, Tibet University, Lhasa, 850000, Tibet, China

<sup>b</sup> School of Geography and Ocean Sciences, Nanjing University, Nanjing, 210023, China

<sup>c</sup> Institute of Global Environmental Change, Xi'an Jiaotong University, Xi'an, 710049, China

<sup>d</sup> Yunnan Key Laboratory of Plateau Geographical Processes and Environmental Changes, Faculty of Geography, Yunnan Normal University, Kunming, 650500, China

<sup>e</sup> Department of Earth Sciences, University of Minnesota, Minneapolis, 55455, MN, USA

<sup>f</sup> State Key Laboratory of Loess and Quaternary Geology, Institute of Earth Environment, Chinese Academy of Sciences, Xi'an, 710077, China

### ARTICLE INFO

#### Keywords:

Southern Tibetan plateau

Stalagmite

Stable isotopes

Indian summer monsoon

Westerlies

### ABSTRACT

Two atmospheric circulation systems, the mid-latitude Westerlies and the Indian summer monsoon (ISM), are key drivers of hydroclimate variability in the Tibetan Plateau (TP). However, the variability of the Westerlies and the ISM in the TP and their relationship remain unclear. Here, we present a new, precisely dated speleothem record from Pumu Cave in the southern TP, spanning the past 339,000 years. The Pumu  $\delta^{18}\text{O}$  record closely tracks Northern Hemisphere summer insolation (NHSI) and aligns with speleothem  $\delta^{18}\text{O}$  records from both the ISM and East Asian Summer Monsoon regimes. In comparison to previous studies, the Pumu  $\delta^{18}\text{O}$  record is primarily interpreted as a proxy indicating the ISM intensity. Furthermore, the orbital-scale variability in Pumu  $\delta^{18}\text{O}$ ,  $\delta^{13}\text{C}$ , and trace element records reveals that the ISM intensity governs effective rainfall in the southern TP. Additionally, the Pumu speleothem growth occurred exclusively during warm, wet interglacial periods, while hiatuses persisted throughout cold, dry glacial periods. This pattern mirrors findings from Tianmen Cave, reinforcing the hypothesis that interglacial temperatures are a prerequisite for speleothem formation in the TP, with strong ISM precipitation, low ice volume and high  $\text{CO}_2$  levels providing sufficient conditions. Besides, differences in growth periods and  $\delta^{18}\text{O}$  amplitudes are also observed between Pumu and Tianmen speleothems, which likely suggest variations in their moisture sources and duration of seasonal ground thaw in different parts of the TP. While the Westerlies-related moisture does not appear to change orbital phases of the  $\delta^{18}\text{O}$  variability in the TP, which follows the NHSI dominantly, it modulates the amplitude of  $\delta^{18}\text{O}$  fluctuations. Finally, the different roles of the ISM and Westerlies suggest that while the ISM controls the hydroclimate dynamic variability, environmental conditions in the southern TP appear to be also influenced by global ice volume and  $\text{CO}_2$  levels, highlighting the complex interplay among these climatic forcings.

### 1. Introduction

The Tibetan Plateau (TP) is considered as the “Third Pole” of the Earth, with an average elevation exceeding 4000 m altitude above sea level (a.s.l.) (Qiu, 2008). This region plays an important role in regulating both the Westerlies and the Asian monsoon system (e.g., An et al., 2001, 2012; Wu et al., 2012; Ye and Wu, 1998). At the same time, the climate in the TP is particularly sensitive to global climate change (Huang et al., 2023; Liu and Chen, 2000; Su et al., 2024; Yao et al., 2019). The TP is also known as “the Asian Water Tower”, serving as the

source of more than ten major rivers in the world (Bolch et al., 2012; Immerzeel et al., 2010, 2020; Yao et al., 2022).

Modern observations show that glaciers across the TP are generally retreating (e.g., Bhattacharya et al., 2021; Miles et al., 2021; Yao et al., 2012, 2022). Specifically, glaciers in the northern TP are shrinking slowly or even expanding slightly (Farinotti et al., 2020; Shean et al., 2020; Yao et al., 2012), whereas glaciers in the southern TP are retreating significantly (Bolch et al., 2012; Yao et al., 2012, 2022). Notably, recent studies suggest that glacier mass loss is now widespread even in the northern TP, mainly driven by temperature rising during

\* Corresponding author. at: Institute of Global Environmental Change, Xi'an Jiaotong University, Xi'an, 710049, China.

E-mail address: [cheng021@xjtu.edu.cn](mailto:cheng021@xjtu.edu.cn) (H. Cheng).

summer (Bhattacharya et al., 2021; Hugonnet et al., 2021). In addition to temperature rising (Bhattacharya et al., 2021; Kraaijenbrink et al., 2017), the regional climate change is also characterized by a contrasting precipitation pattern across the TP: decreasing precipitation in the south and increasing in the north, driven by shifts in atmospheric circulation, particularly a weakening Indian summer monsoon (ISM) and strengthened Westerlies, respectively (Thompson et al., 2018; Yao et al., 2012, 2022). Meteorological observations further indicate that most of the TP has become warmer and wetter in recent decades, except for the southern TP, which manifests a warmer and drier trend (Yang et al., 2014; Liu et al., 2021). While projections suggest that total lacustrine areas in the northern TP could double by 2100, driven by increased precipitation and glacier meltwater (Xu et al., 2024), lakes in the southern TP have shown a persistent decreasing trend (Lei et al., 2014; Liu et al., 2021; Zhang et al., 2020), attributed largely to decreases in summer precipitation (Liu et al., 2021; Zhang et al., 2020).

Generally, the TP receives precipitation mainly from two sources: the ISM, a subsystem of the Asian summer monsoon (ASM), and the mid-latitude Westerlies (e.g., An et al., 2001, 2012; Tian et al., 2001, 2003; Yao et al., 2013). Specifically, the southern TP (south of 30°N) is distinguished as the “monsoon domain”, the northern TP (north of 35°N) as the “westerlies domain”, and the region between 30°N and 35°N as the transition domain, where influences of the Westerlies and the ISM alters (Fig. 1) (Yao et al., 2013). Precipitation oxygen isotope ratio ( $\delta^{18}\text{O}_\text{p}$ ) records from the Westerlies domain exhibit a strong link between the  $\delta^{18}\text{O}_\text{p}$  and local temperature, while precipitation amount has little influence (Yao et al., 2013). Conversely, in the monsoon domain,  $\delta^{18}\text{O}_\text{p}$  is inversely correlated with precipitation amount (Yao et al., 2013). However, a recent study suggests that the amount effect contributes little to the  $\delta^{18}\text{O}_\text{p}$  variability, and instead, changes in rainout of water vapor during the transport are the main driver of the  $\delta^{18}\text{O}_\text{p}$  variability in the monsoon domain (Man et al., 2022). Furthermore, global atmospheric general circulation models suggest that precipitation in the monsoon domain is predominantly sourced from the moisture originating in South Asia and the Indian Ocean, followed by contributions from East Asia (Man et al., 2022). Meanwhile, the Westerlies are

identified as the primary moisture source for precipitation in the Westerlies domain (Man et al., 2022), with notable contributions from South Asia and the Indian Ocean as well (An et al., 2017; Man et al., 2022; Ramisch et al., 2016). Terrestrial moisture also significantly influences precipitation over the TP (Cheng et al., 2024; Y. Li et al., 2022). Collectively, as an integrated tracer of atmospheric processes at different spatial scales,  $\delta^{18}\text{O}_\text{p}$  provides valuable information about local temperature, precipitation amount, moisture sources, and transport pathways (Dansgaard, 1964). Consequently,  $\delta^{18}\text{O}_\text{p}$  is widely used as a proxy for reconstructing past climate variations across various temporal and spatial scales.

However, the interpretation of  $\delta^{18}\text{O}$  from different climate archives from the TP remains controversial. For example,  $\delta^{18}\text{O}$  records from ice cores in the Westerlies domain of the TP show correlations with the surface temperature (e.g., An et al., 2016; Hou et al., 2019; Pang et al., 2020; Thompson et al., 1997, 2003, 2018; Tian et al., 2006; Wang et al., 2006; Yao et al., 1997, 2007; Yu et al., 2021). In contrast,  $\delta^{18}\text{O}$  in ice cores from ISM-influenced regions primarily reflects precipitation variability (e.g., Joswiak et al., 2010; Kaspari et al., 2007; Pang et al., 2014; Vuille et al., 2005; Zhang et al., 2005). In addition, a new study suggests that the ice core  $\delta^{18}\text{O}$  records mainly reflects warming in the middle and upper troposphere over the south of the TP rather than the low land surface temperature changes (Li et al., 2025). Notably, the new Guliya ice core record challenges the assumption that the  $\delta^{18}\text{O}$  primarily reflects temperature in the northern TP (Thompson et al., 2022). Instead, a recent study shows that orbital-scale similarities between summer insolation and the new Guliya ice core  $\delta^{18}\text{O}$  suggest that isotopic fractionation in northern TP precipitation was largely controlled by summer temperature (Thompson et al., 2024). Intriguingly, the new Guliya ice core record is in-phase with speleothem  $\delta^{18}\text{O}$  records (reflecting monsoon intensity) from the ASM region during glacial periods and the Holocene (Thompson et al., 2022, 2024), likely pointing to a common mechanism linked to large-scale atmospheric circulation changes between the ASM and the Asian Westerlies (AW) (e.g., Cheng et al., 2012b, 2016b; H. Wang et al., 2022). However, the consistency of the new Guliya ice core  $\delta^{18}\text{O}$  with Northern Hemisphere summer insolation

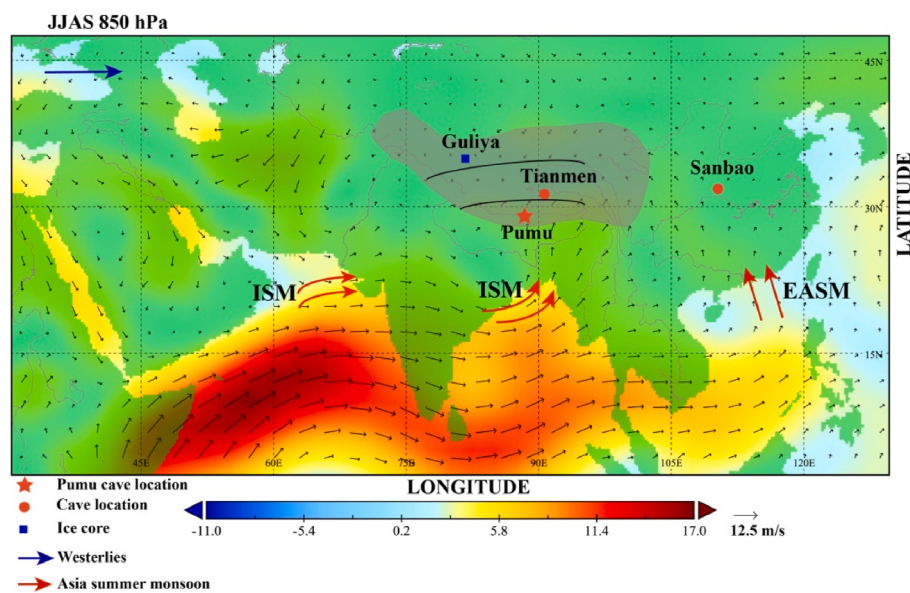


**Fig. 1.** Location of the study site and averaged wind field isobars at 850 hPa in summer (June to September) from 1980 to 2024 (A.D.). Arrows depict the predominant wind directions of the Indian summer monsoon and East Asia summer monsoon in red, and the Westerlies in blue. The grey shaded area denotes topography above 3000 m a.s.l., delineating the TP. The red star marks Pumu Cave, 29°18' N, 88°30' E, ~4920 m a.s.l. Locations of other referenced records include Tianmen Cave (30°55' N, 90°4' E, ~4800 m a.s.l., Cai et al., 2010, 2012; H. Wang et al., 2022), Sanbao Cave (31°40' N, 110°26' E, ~1900 m a.s.l., Cheng et al., 2016a), and the Guliya ice core (35°5' N, 81°29' E, ~6200 m a.s.l., Thompson et al., 2024). Black lines show schematic boundaries separating the three domains: the westerlies domain, the transition domain, and the monsoon domain (modified from Yao et al., 2013). (For interpretation of the references to color in this figure legend, the reader is referred to the Web version of this article.)

(NHSI) on the orbital-scale remains questionable, particularly during the MIS2 period. The  $\delta^{18}\text{O}$  records of stalagmites in the East Asian summer monsoon (EASM, another major subsystem of the ASM) region show a progressively more positive trend as NHSI decreased during the MIS2 period. In contrast, the  $\delta^{18}\text{O}$  records of the new Guliya ice core presented an opposite pattern (Fig. S1). Speleothem  $\delta^{18}\text{O}$  records from the transition domain of the TP further highlight the ISM influence, suggesting that precipitation is the primary driver of the speleothem  $\delta^{18}\text{O}$  variability on orbital to millennial timescales (e.g., Cai et al., 2010, 2012; Y. W. Li et al., 2022; H. Wang et al., 2022). Furthermore, the Benle  $\delta^{18}\text{O}$  record, located at the intersection of ISM and EASM in the TP, also shows a consistent correspondence with the monsoon intensity on millennial timescales (Han et al., 2017). Taken together, these observations underscore the complexity in interpreting the  $\delta^{18}\text{O}$  across the TP. Particularly, the mechanisms and variations of precipitation  $\delta^{18}\text{O}$  under the synergistic effect of the AW and ISM over the TP remain unclear, especially on orbital-scales.

In this study, we present a new high-resolution, absolutely dated speleothem  $\delta^{18}\text{O}$  record from Pumu Cave in the monsoon domain of the TP, spanning the past  $\sim 339$  ka (thousand years). Our goal is to identify the dominant factors influencing speleothem  $\delta^{18}\text{O}$  on orbital and glacial-interglacial timescales in the southern TP, and in turn to explore the underlying mechanisms driving divergences in  $\delta^{18}\text{O}$  signals and possible links to different moisture sources.

## 2. Materials and methods

### 2.1. Cave, sample and modern climatology

Pumu Cave ( $29^{\circ}18' \text{N}$ ,  $88^{\circ}30' \text{E}$ ,  $\sim 4920$  m a.s.l.) is located in the Sangzhu District of Shigatse City, Xizang Autonomous Region, China, south of the Yarlung Zangbo River (Fig. 1). The cave, developed in Cretaceous to Tertiary limestone, is located on a bare mountainside, characterized by sparse vegetation (Wei, 1994). The stalagmite sample (PM-1) was collected in 2023 from a small hall in the cave. This  $\sim 7.2$  cm-long stalagmite, composed of light brown calcite, was cut along the growth axis using a thin diamond blade and then polished.

The region receives an average annual precipitation of  $\sim 285.5$  mm, based on data (1957–2020) from the Jiangzi meteorological station ( $\sim 4000$  m a.s.l.) approximately  $\sim 100$  km from Pumu Cave. Over 90 % of local precipitation falls in summer months (June–September) during the ISM (Fig. S2). The mean annual temperature is  $5^{\circ}\text{C}$ , with the warmest months (June–September) averaging  $12^{\circ}\text{C}$ .

To investigate moisture sources, we applied the Hybrid Single-Particle Lagrangian Integrated Trajectory model (HYSPLIT) (Stein et al., 2015) to calculate air mass back trajectories. The analysis identified three main trajectory categories for Pumu Cave, with most air parcels originating from the Bay of Bengal (BOB) and the southern Indian Ocean. Additionally, continental recycling was identified as a significant moisture source (Fig. S3). Modern observational data confirm a notable decrease in precipitation  $\delta^{18}\text{O}$  during the summer months in the monsoon domain of the southern TP (Tian et al., 2001; Yao et al., 2013; Yu et al., 2008).

### 2.2. $^{230}\text{Th}$ dating and stable isotope analysis

A total of seventeen  $^{230}\text{Th}$  dates of PM-1 (Table S1) were measured at Xi'an Jiaotong University, China, using a multi-collector inductively coupled plasma mass spectrometer (MC-ICP-MS) (Thermo-Finnigan Neptune Plus) and an improved  $^{230}\text{Th}$  dating technique (Cheng et al., 2013). We used standard chemistry procedures to separate uranium and thorium for dating (Edwards et al., 1987; Cheng et al., 2013). All age uncertainties are reported at the  $2\sigma$  level.

724 sub-samples were drilled for oxygen and carbon isotope ( $\delta^{18}\text{O}$  and  $\delta^{13}\text{C}$ ) analyses using a digitally controlled tri-axial micromill equipped with a 0.5 mm carbide dental burr. Subsampling intervals

were set at 100  $\mu\text{m}$  along the stalagmite growth axis to achieve high-temporal-resolution data. Isotopic measurements were conducted on a Finnigan MAT-253 mass spectrometer coupled with an online carbonate preparation system (Kiel-IV) at the Isotope Laboratory, Xi'an Jiaotong University. Results are reported relative to the Vienna Pee Dee Belemnite (VPDB) standard, with a precision of 0.1 ‰ at the  $1\sigma$  level.

Trace element measurements of PM-1 were determined using Laser-Induced Breakdown Spectroscopy (LIBS) at the Isotope Laboratory, Xi'an Jiaotong University, following the method detailed in H. Li et al. (2018).

### 2.3. Age model

Among the 17  $^{230}\text{Th}$  dates of PM-1, 12 (71 %) have relatively small uncertainties (<1 %) for ages younger than 300 ka BP (before present, where present = 1950 CE). These ages are stratigraphically consistent within uncertainties. An age-depth model was constructed using OxCal v4.4 (Bronk Ramsey, 2008) (Fig. S4).

## 3. Results

The dating results of stalagmite PM-1 show that its growth spans several time intervals: 339 - 315 ka BP, 246 - 238 ka BP, 223 - 217 ka BP, and 127 - 118 ka BP (Fig. S4). Growth rates vary from 0.5 to 4.8  $\mu\text{m}/\text{yr}$ , with mean rates of 0.8  $\mu\text{m}/\text{yr}$  (132-yr resolution) during 339 - 315 ka BP, 4.8  $\mu\text{m}/\text{yr}$  (21-yr resolution) during 246 - 238 ka BP, 1.7  $\mu\text{m}/\text{yr}$  (60-yr resolution) during 223 - 217 ka BP, and 0.5  $\mu\text{m}/\text{yr}$  (179-yr resolution) during 127 - 118 ka BP.

Using micromill sampling, the stable isotope time series achieved mean temporal resolutions ranging from 21 to 179 years. The  $\delta^{18}\text{O}$  values vary from  $-14.83$  ‰ to  $-24.41$  ‰, with a total amplitude of 9.58 ‰, covering Marine Isotope Stages (MIS) 5e, 7c, 7e, 9c, 9d and 9e (Fig. 2). Speleothem growth in PM-1 preferentially occurred during warm and wet interglacial periods, while hiatuses correspond to cold and dry glacial periods, consistent with previous records from Tianmen Cave (H. Wang et al., 2022).

The  $\delta^{13}\text{C}$  values exhibit an overall amplitude of 8.57 ‰, ranging from 1.65 to  $-6.92$  ‰, and display the variability closely mirroring that of the  $\delta^{18}\text{O}$ . In addition, the trace element ratios (i.e., Mg/Ca, Sr/Ca and Ba/Ca) generally exhibit coherent patterns, both among themselves as well as in comparison with the  $\delta^{18}\text{O}$  and  $\delta^{13}\text{C}$  records (Fig. 4). Although resolutions of the trace element data are relatively low, broad correlations are evident on orbital-scales.

## 4. Discussion

### 4.1. Interpretation of the speleothem $\delta^{18}\text{O}$

The replications of isotopic records from the same or nearby caves can provide a robust test on whether the stalagmite formation was under an isotopic equilibrium condition (e.g., Cheng et al., 2006; Dorale and Liu, 2009; Dykoski et al., 2005; Wang et al., 2008). The broad consistency between the PM-1  $\delta^{18}\text{O}$  record and other  $\delta^{18}\text{O}$  records across the TP and the ASM domain suggests a common climatic mechanism influencing the  $\delta^{18}\text{O}$  variability on orbital-scales (Figs. 2 and 3). Generally,  $\delta^{18}\text{O}$  values of stalagmite carbonates are essentially controlled by the isotopic composition of drip water and cave temperature (Hendy and Wilson, 1968). However, the large amplitude (9.58 ‰) in the PM-1  $\delta^{18}\text{O}$  record cannot be attributed solely to temperature changes, as this would imply unrealistically large fluctuations exceeding  $\sim 38^{\circ}\text{C}$  (assuming  $\sim -0.25\text{‰/}^{\circ}\text{C}$ ; O'Neil et al., 1969). Instead, the observed  $\delta^{18}\text{O}$  variability is more plausibly attributed to changes in the meteoric precipitation  $\delta^{18}\text{O}$  (Cai et al., 2010, 2012; H. Wang et al., 2022).

Previous studies suggest that the  $\delta^{18}\text{O}$  variability of precipitation across the vast ASM domain is largely governed by the intensity of the

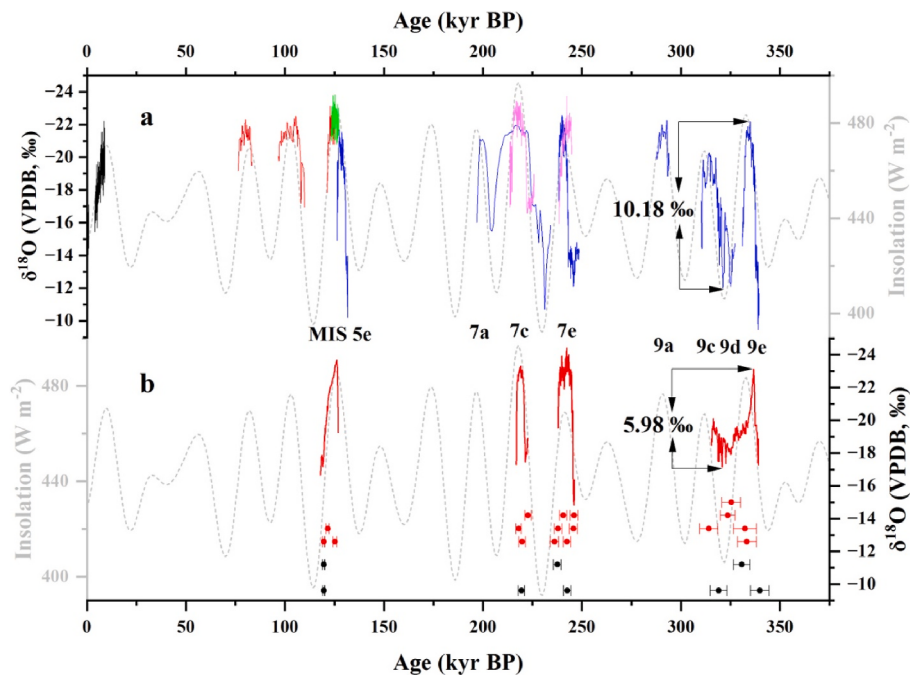


**Fig. 2.** Comparison of the Pumu Cave  $\delta^{18}\text{O}$  record with the Tianmen Cave  $\delta^{18}\text{O}$  record. (a) Tianmen Cave  $\delta^{18}\text{O}$  composite record, represented by five stalagmites in different colors, as follows: Black, TM-18 (Cai et al., 2012); Red: TM-2; Green: TM-5 (Cai et al., 2010); Blue: 19TM-3; Pink: 19TM-5 (H. Wang et al., 2022). (b) Pumu Cave  $\delta^{18}\text{O}$  record (PM-1, this study). Both records are plotted on 21 July insolation at 65 °N (grey dotted line) (Berger, 1978). The red (black) bars below represent the  $^{230}\text{Th}$  age data from PM-1 (PM-2), with  $2\sigma$  uncertainties. Arrows highlight the amplitude of speleothem  $\delta^{18}\text{O}$  changes. Marine Isotope Stages (MISs) are also indicated. (For interpretation of the references to color in this figure legend, the reader is referred to the Web version of this article.)

summer monsoon, driven by large-scale atmospheric circulation changes. These factors include rainfall amount, temperature, seasonality, as well as shifts in moisture source and trajectory (e.g., Battisti et al., 2014; Bosmans et al., 2018; Chen and Li, 2018; Cheng et al., 2012a, 2012b, 2016a, 2019, 2022; Hu et al., 2019; Liang et al., 2024; Pausata et al., 2011; Tabor et al., 2018; Wang et al., 2008; Xue et al., 2023; Yuan et al., 2004; Zhang and Li, 2019; Zhang et al., 2021). On orbital to millennial timescales, speleothem  $\delta^{18}\text{O}$  in the TP is widely interpreted as a proxy for paleomonsoon intensity (e.g., Cai et al., 2010, 2012; Y. W. Li et al., 2022; H. Wang et al., 2022). Specifically, increased moisture from ISM sources results in more negative precipitation  $\delta^{18}\text{O}$  values, consistent with previous findings (e.g., Cai et al., 2010, 2012; Cai et al., 2017; He and Richards, 2016; Y. W. Li et al., 2022; Man et al., 2022; Tian et al., 2001; H. Wang et al., 2022; Yao et al., 2009, 2013; Yu et al., 2008). We therefore interpret the stalagmite  $\delta^{18}\text{O}$  from Pumu Cave as a proxy for the ISM intensity in the region, with higher values indicating a weakened ISM, and vice versa, in line with most previous studies (e.g., Cai et al., 2010, 2012; Y. W. Li et al., 2022; H. Wang et al., 2022).

#### 4.2. Hydroclimate variation across glacial-interglacial cycles

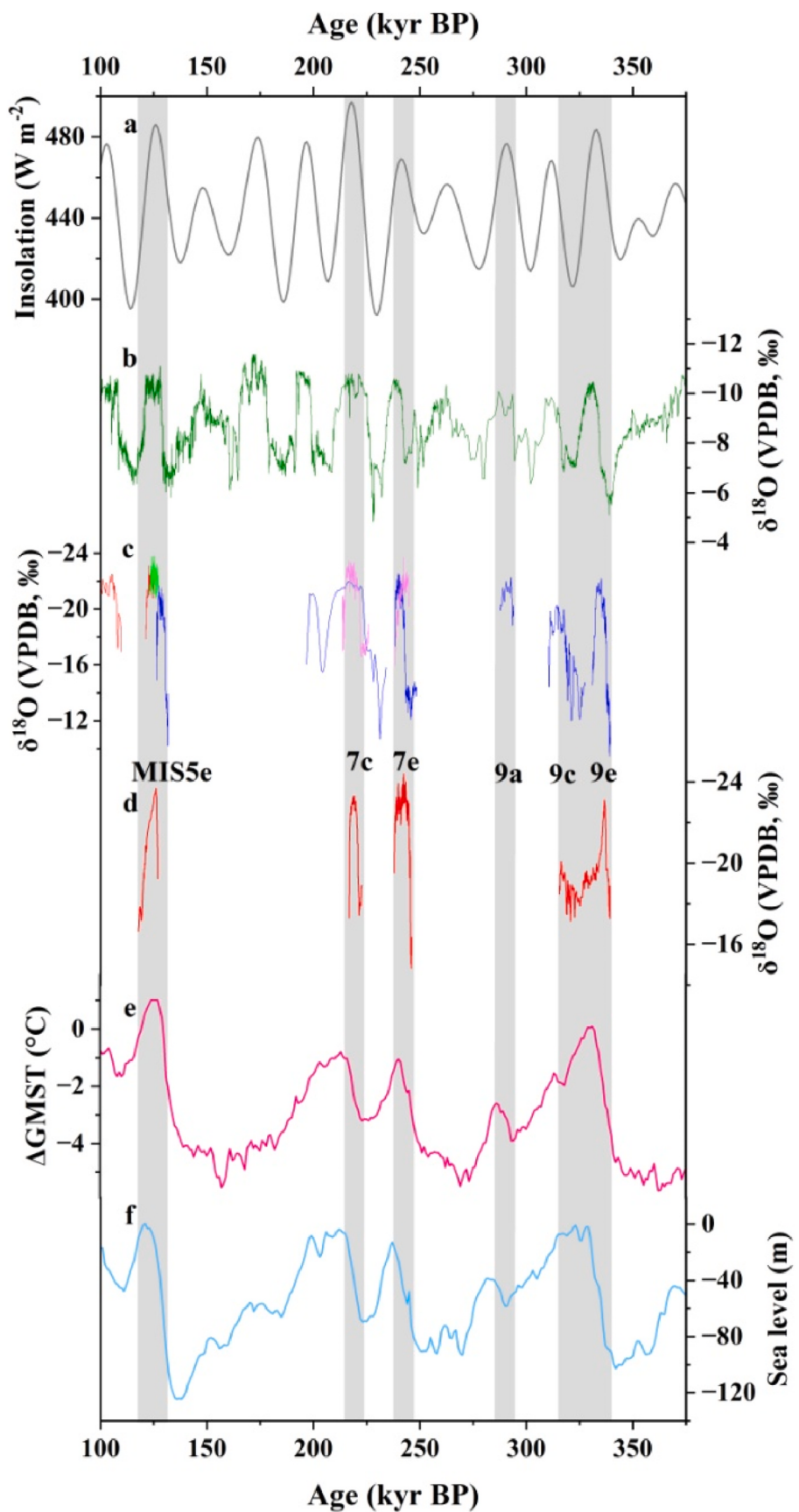
Stalagmite growth in Pumu Cave generally occurred during warm interglacial periods (Fig. 3), consistent with findings from Tianmen Cave and travertine formations over the TP (e.g., Meyer et al., 2017; H. Wang et al., 2022; Z. Wang et al., 2016, 2022; Zentmyer et al., 2008). This observation suggests that interglacial temperature condition acts as a prerequisite for speleothem growths and travertine formations, with strong ISM precipitation providing an additional hydrological requirement (H. Wang et al., 2022). In addition, a recent study suggests that the overlying permafrost conditions may be the primary drivers of speleothem growth during glacial terminations (Yan et al., 2025). The PM-1  $\delta^{18}\text{O}$  record resembles the EASM (Cheng et al., 2016a) and Tianmen records (H. Wang et al., 2022) on orbital-scales, closely tracking NHSI and thus supporting the causal link between insolation forcing and

summer monsoon intensity (Kutzbach, 1981).

A notable exception is observed during MIS9a, when high NHSI does not correspond with any speleothem growth in Pumu Cave (Figs. 2 and 3). This hiatus coincides with a smaller increase in the Global Mean Surface Temperature difference from the late Holocene (i.e., 0 °C at 0 ka) ( $\Delta\text{GMST}$ ) and a relatively minor sea-level rise during MIS9a (Fig. 3e and f). Notably, a slow stalagmite growth persisted in Tianmen Cave during this interval (Fig. 3c), in contrast to the growth hiatus at Pumu Cave (Fig. 3d). Both speleothems from Pumu Cave cover nearly identical age ranges (Fig. 2b). In other words, our new stalagmite data highlights that the growth periods in Pumu Cave are only associated with significant  $\Delta\text{GMST}$  increases and/or sea-level rises (Fig. 3).

The absence of speleothem growth at Pumu Cave during MIS9a may reflect either insufficient duration of climate amelioration to resume the growth or the influence of non-climatic factors, such as aquifer re-routing (Klose et al., 2024). Assuming the freezing temperature was not a constraint, as the speleothem growth was found at Tianmen Cave in the transition zone of the TP, the relatively reduced ISM precipitation is then likely the factor limiting the speleothem growth in Pumu Cave in the monsoon domain in the TP. Conversely, in the transition zone of the TP, the AW-derived winter moisture significantly enhanced the precipitation in the area (Yao et al., 2013). Therefore, the Pumu Cave speleothem growth primarily reflects the ISM intensity, in addition to the  $\Delta\text{GMST}$ , which is different from the speleothem growth in the transition domain in the TP. As such, this observation supports the hypothesis that interglacial temperatures set the stage for speleothem growth in the TP, with strong ISM precipitation as the enabling factor (H. Wang et al., 2022).

During MIS9a, the Tianmen speleothem grew over a relatively short period (~6.3 ka), depositing a thin layer (3.2 mm) at a slow growth rate of 0.5  $\mu\text{m}/\text{yr}$  (H. Wang et al., 2022). Despite a peak in NHSI suggesting a brief warm phase, the lack of Pumu Cave speleothem growth implies weaker ISM intensity compared to MIS9c and MIS9e. This observation suggests a critical role of precipitation in speleothem formation, even during periods of high NHSI. Furthermore, the anti-phase relationship



(caption on next page)

**Fig. 3.** Comparison of the Pumu Cave  $\delta^{18}\text{O}$  record with global climate proxies. (a) 21 July insolation at 65 °N (Berger, 1978). (b) Asian Monsoon composite record (Cheng et al., 2016a). (c) Tianmen Cave  $\delta^{18}\text{O}$  composite record, represented by four stalagmites in different colors, as follows: Red: TM-2; Green: TM-5 (Cai et al., 2010); Blue: 19TM-3; Pink: 19TM-5 (H. Wang et al., 2022). (d) Pumu Cave  $\delta^{18}\text{O}$  record (this study). (e) Global mean surface temperature differences ( $\Delta\text{GMST}$ ) relative to the late Holocene (i.e., 0 °C at 0 ka) (Clark et al., 2024). (f) Composite global sea level record (Spratt and Lisicki, 2016). Grey shading highlight periods of speleothem growth, which occurred exclusively during warm and wet interglacial periods. Marine Isotope Stages (MISs) are also indicated. (For interpretation of the references to color in this figure legend, the reader is referred to the Web version of this article.)

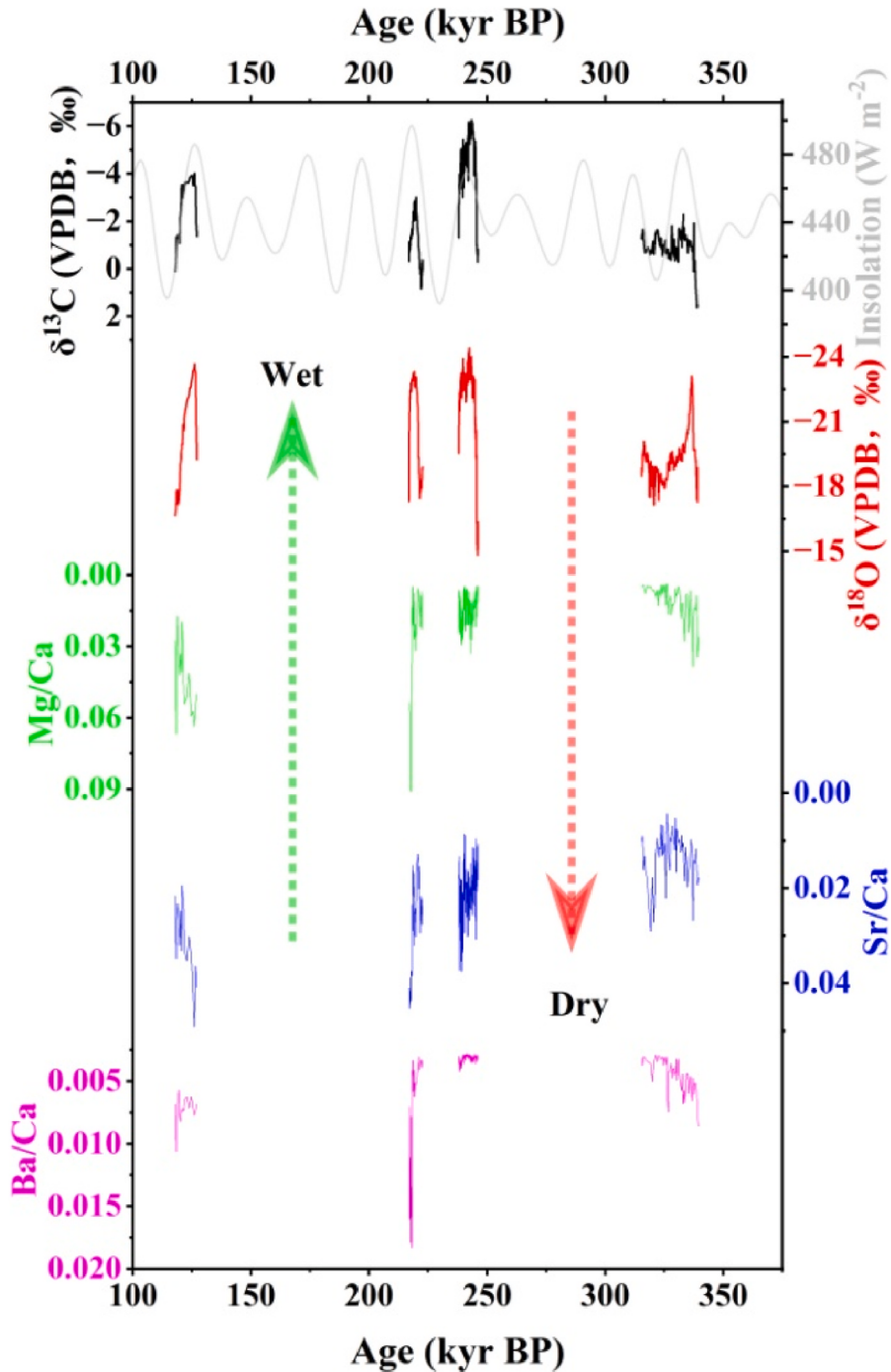


**Fig. 4.** Comparison of Pumu trace element (Mg/Ca, Sr/Ca and Ba/Ca) data with the stable isotope profile. The grey line indicates 21 July insolation at 65 °N (Berger, 1978). The Pumu  $\delta^{13}\text{C}$  record is broadly in phase with both trace element ratios and  $\delta^{18}\text{O}$ , but anti-phased respect to NHSI on orbital timescales, indicating that both stable isotopes and trace element records were affected by a common mechanism on orbital timescales, linked to changes in local effective rainfall modulated by ISM intensity.

between the AW and ASM climates on glacial-interglacial and millennial timescales indicates that the Westerlies contributed significant moisture during cold periods when the ASM weakened (An et al., 2012). This interplay between the AW and the ASM modulates hydroclimate pattern and variability in the TP. We also observed a same phenomenon during MIS7a (Fig. 2), suggesting that the ISM might be weakened relatively near the end of interglacial periods, even NHSI was at a precession peak. This scenario may be attributed to the considerable increase in global ice volume near the end of the interglacial period (Fig. 3), suggesting that hydroclimate variations in the southern TP may also respond to changes in the global ice volume.

Notably, in the Tianmen record, the  $\delta^{18}\text{O}$  values during MIS9a are considerably more negative than during MIS9c, and are in phase with NHSI (H. Wang et al., 2022). This may suggest a stronger ISM in terms of dynamic (or circulation), while weaker thermodynamic due to less moisture under presumably lower temperature condition during MIS9a compared to MIS9c. In that regard, speleothem growths in Tianmen Cave during MIS9a may suggest a contribution of the AW moisture, which is likely compensated partially for the reduced ISM moisture in the transition domain. On the other hand, the inverse  $\delta^{18}\text{O}$ -NHSI relationship at the precession band across both monsoon and transition domains of the TP indicates a common dynamic mechanism, likely driven by large-scale atmospheric circulation changes on orbital-scales. This pattern further suggests that AW- and ISM-derived moistures show similar orbital-scale patterns in terms of  $\delta^{18}\text{O}_\text{p}$  over the TP (e.g., Cheng et al., 2012b; H. Wang et al., 2022).

#### 4.3. Amplitude differences in precipitation $\delta^{18}\text{O}$ variations between the monsoon and the transitional domains in the TP

Unlike MIS5 and MIS7, the Pumu speleothem grew continuously during MIS9, spanning a full precession cycle, including the interval MIS9d, when the ISM was presumably weaker under a lower NHSI condition (Fig. 2). This observation allows us to compare the amplitude of our Pumu  $\delta^{18}\text{O}$  record with the Tianmen record across an entire precession cycle. Apparently, the Pumu amplitude (5.98‰) is significantly smaller than that of the Tianmen record (10.18‰) over the same precessional cycle. While the minimum  $\delta^{18}\text{O}$  values in the Tianmen and Pumu cave records are essentially comparable during MIS9e to 9c (−22.18‰ vs. −23.12‰), the primary difference stems from their maximum  $\delta^{18}\text{O}$  values (−12.00‰ vs. −17.14‰) (Fig. 2). Specifically, the Tianmen record shows much higher  $\delta^{18}\text{O}$  values during the lower half of NHSI at the precession band, corresponding to the period when the ISM was likely weaker.

One plausible explanation for the higher  $\delta^{18}\text{O}$  values in the Tianmen record than in the Pumu record is the difference in their moisture sources. Modern meteorological data reveal that over 90% of annual precipitation at the Pumu Cave site occurs during the summer months (June–September), driven predominantly by the ISM (Figs. S2 and S3). In contrast, winter months (November–February) contribute only 0.6% of annual precipitation under the influence of the AW. The Tianmen Cave site, however, receives approximately 3% of its annual precipitation during winter. The ISM-driven rainfall in summer typically has low  $\delta^{18}\text{O}$  values, while the moisture from the AW tends to have relatively high  $\delta^{18}\text{O}$  (e.g., Cai et al., 2017; He and Richards, 2016; Tian et al., 2001; Yao et al., 2009, 2013; Yu et al., 2008). Therefore, the differences in the isotopic composition between these sources (Yao et al., 2009, 2013) may amplify the  $\delta^{18}\text{O}$  variability at Tianmen Cave. In this regard, the Pumu  $\delta^{18}\text{O}$  record would be a more direct (or ‘purer’) indicator of ISM dynamics, with the minimal interference from alternative moisture sources.

A second factor influencing  $\delta^{18}\text{O}$  amplitude differences between the two sites is the seasonal bias of infiltration, governed by variations in annual ground thaw duration (Batchelor et al., 2024). The availability of liquid water for infiltration depends on the thawing of frozen soil, snow, and ice. In colder regions, winter snowmelt that occurs before ground

thaw typically contributes to runoff rather than infiltration (Pavoni et al., 2023). During colder periods, prolonged freezing conditions reduce the contribution of  $^{18}\text{O}$ -enriched winter precipitation from the AW to dripwater in caves. This effect is especially pronounced at Pumu Cave, where winter precipitation is negligible. In contrast, the Tianmen Cave site, with lower mean annual temperature and more winter precipitation, has a longer frost season (Fig. S2). Under this condition, it is possible that a longer duration of annual ground thaw process would be favorable to increases in the contribution of the cold-season precipitation to the cave dripwater, resulting in higher speleothem calcite  $\delta^{18}\text{O}$  values (Batchelor et al., 2024). This dynamic effect contributes to higher  $\delta^{18}\text{O}$  variability in the Tianmen record, particularly during the lower half of NHSI precession cycles.

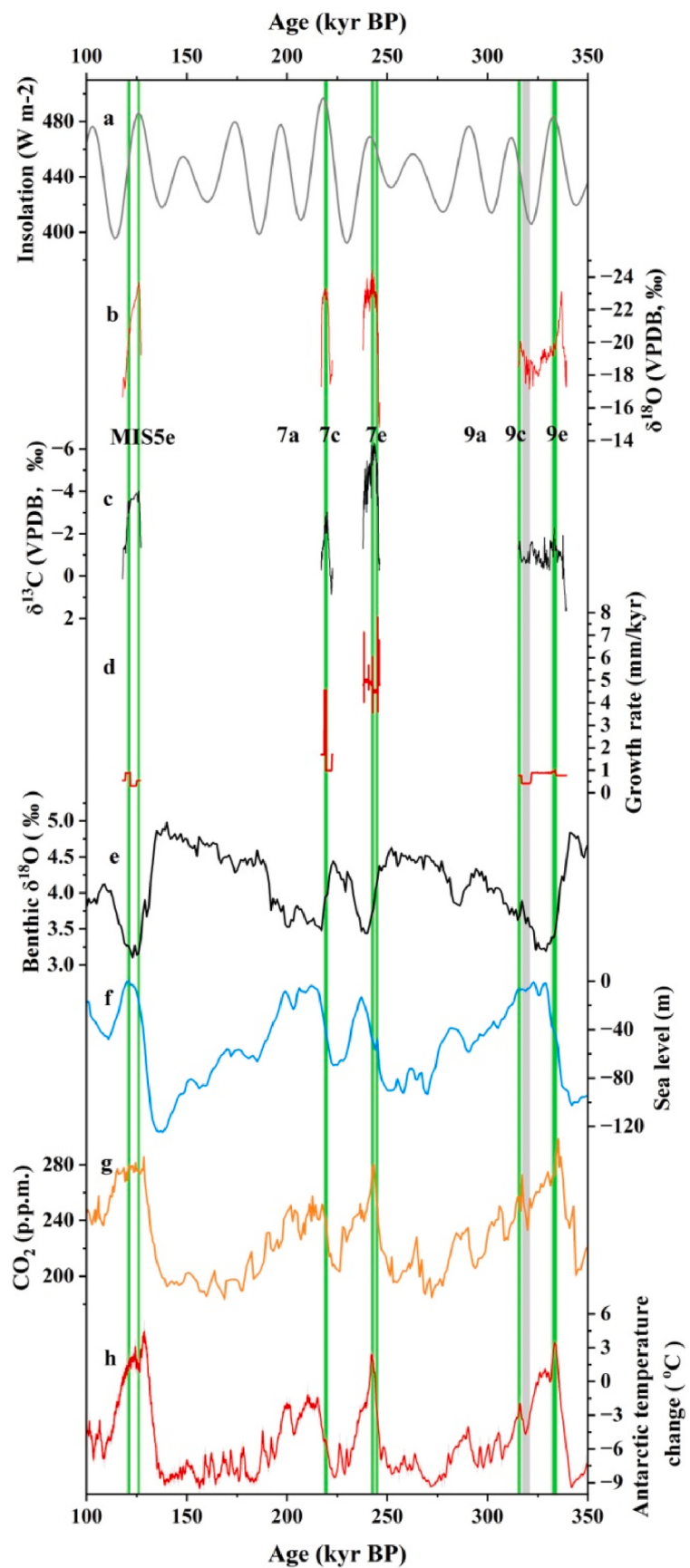
Considering above mechanisms, differences in  $\delta^{18}\text{O}$  amplitude between Pumu Cave in the monsoon domain and Tianmen Cave in the transition domain likely arises from their differences in moisture sources and the duration of seasonal ground thawing. This explanation aligns with the observation that Tianmen  $\delta^{18}\text{O}$  values are only 0.94‰ heavier than Pumu  $\delta^{18}\text{O}$  values during the peaks of the NHSI precession cycle, but are 5.14‰ heavier during the lower half of the precession cycles.

#### 4.4. Further evidence of orbital controls on the local environment

Trace element ratios in speleothems, such as Mg/Ca, Sr/Ca, and Ba/Ca, have emerged as valuable proxies for reconstructing past hydroclimatic changes across various timescales (e.g., Bernal et al., 2016; Cheng et al., 2016b; Hartmann et al., 2013; Kaushal et al., 2024; Liu et al., 2020; Pérez-Mejías et al., 2021; Springer et al., 2008; Warken et al., 2018; Zhang et al., 2018). Correlations among these proxies are often attributed to the dominant effect by the prior calcite precipitation (PCP) processes (e.g., Allan et al., 2018; Baldini et al., 2006; Cheng et al., 2016b; Cruz et al., 2007; Fairchild and Treble, 2009; Fairchild et al., 2000; Griffiths et al., 2010; Johnson et al., 2006; Owen et al., 2016; Treble et al., 2003; Vansteenberge et al., 2020; Verheyden et al., 2000), supported by numerous cave monitoring studies (e.g., Fairchild et al., 2000; Johnson et al., 2006; Lyu et al., 2023; Musgrove and Banner, 2004; Olson et al., 2024; Oster et al., 2021; Tremaine and Froelich, 2013; Wong et al., 2011; Zhang and Li, 2019). In addition,  $\delta^{13}\text{C}$  values in karst systems are another important indicator of local environmental changes, reflecting variations in soil processes and vegetation cover, linked to regional hydrological conditions (e.g., Chen et al., 2021a, 2021b; Fohlmeister et al., 2020; Lechleitner et al., 2017; T. Li et al., 2018). In many cases, coupled variations in speleothem trace element ratios and  $\delta^{13}\text{C}$  are largely governed by a number of common processes, including effective infiltration, soil and vegetation dynamics, and hydrological changes at the cave site (e.g., Baker et al., 1997; Breitenbach et al., 2015; Cheng et al., 2016b; Fohlmeister et al., 2020; Lechleitner et al., 2017; Li et al., 2021; Pérez-Mejías et al., 2019; Wu et al., 2023).

A positive correlation is observed between PM-1 trace element ratios (Mg/Ca, Sr/Ca, Ba/Ca) and  $\delta^{13}\text{C}$ , suggesting a central role of the PCP processes. As shown in Fig. 4, the Pumu  $\delta^{13}\text{C}$  record is broadly in phase with both trace element and  $\delta^{18}\text{O}$  records, and follows NHSI on orbital timescales. This observation implies that wetter conditions in the Pumu Cave area are to first order characterized by lower values in the  $\delta^{13}\text{C}$ , trace element ratios, and  $\delta^{18}\text{O}$ . Hence,  $\delta^{13}\text{C}$  and trace element ratios, along with  $\delta^{18}\text{O}$ , provide consistent evidence that the high NHSI drives the stronger ISM, resulting in generally wetter conditions at the cave site. This observation aligns with the conventional understanding that effective rainfall is linked to orbital-scale monsoon variability in the southern TP.

For each growth phase of PM-1, we also found that higher growth rates correspond to lower  $\delta^{13}\text{C}$  values, and vice versa. These periods of higher growth rates tend to coincide with fast declines in global ice volume (or increases in global sea level), rising atmospheric CO<sub>2</sub> concentrations, and warming Antarctic temperature (Fig. 5). Generally, warmer temperature during interstadials and interglacials would



(caption on next page)

**Fig. 5.** Comparison of the PM-1 growth rate with global climate proxies. (a) 21 July insolation at 65 °N (Berger, 1978). (b) Pumu Cave  $\delta^{18}\text{O}$  record. (c) Pumu Cave  $\delta^{13}\text{C}$  record. (d) PM-1 growth rate. (e) LR04 Benthic  $\delta^{18}\text{O}$  stack (Lisiecki and Raymo, 2005). (f) Composite global sea level record (Spratt and Lisiecki, 2016). (g) Relative composite CO<sub>2</sub> record from Antarctic EDC ice core records (Bereiter et al., 2015). Ice core ages follow EDC3 chronology (Parrenin et al., 2007). (h) Relative temperature records from Antarctic EDC ice core record (Jouzel et al., 2007), ice core ages follow EDC3 chronology (Parrenin et al., 2007). Vertical bars illustrate a broad correlation between PM-1 growth rate and global climate proxies. Marine Isotope Stages (MIS) are also indicated.

increase soil respiration rates and soil CO<sub>2</sub>, thereby accelerating rock dissolution rates. This process enhances bedrock dissolution, producing drip water with a higher degree of oversaturation and promoting higher stalagmite growth rates (Pérez-Mejías et al., 2025). The PM-1 record shows the lowest  $\delta^{13}\text{C}$  and the fastest growth rate during MIS7e, suggesting substantial soil development that might have supported strong vegetation activity, increasing soil CO<sub>2</sub>, enhancing bedrock dissolution, and promoting higher speleothem growth rates (Pérez-Mejías et al., 2025). It is worth noting that this behavior does not match up with the pattern of NHSI peaks in the precession orbital-cycle, since the NHSI peak at MIS7c is not the highest (Fig. 5). Thus, it seems that the orbital variations of NHSI, controlling the ISM intensity (dynamic) and consequently  $\delta^{18}\text{O}$ , are not directly responsible for local soil and vegetation changes (Cheng et al., 2022; Zhao et al., 2023). Theoretically, the local hydroclimate changes or monsoon thermodynamics may also be response to global temperature to varying extent linked to the atmospheric CO<sub>2</sub>, the global ice volume and Antarctic temperature variations. The underlying mechanism of the lowest  $\delta^{13}\text{C}$  may be more complex and likely a non-linear response to orbital forcings, which requires further investigations in future.

## 5. Conclusions

The new speleothem  $\delta^{18}\text{O}$  record from Pumu Cave in the southern TP manifests a pattern coherent with speleothem  $\delta^{18}\text{O}$  records from both the ISM and EASM regimes over the past ~339 ka, which closely tracks NHSI on orbital-scales. This coherence underscores the reliability of TP speleothem  $\delta^{18}\text{O}$  as a proxy indicating the ISM intensity. The exceptionally large  $\delta^{18}\text{O}$  amplitude (~9.58‰) observed in the Pumu speleothem on the precession timescale suggests an amplification of precipitation  $\delta^{18}\text{O}$  signals in high altitude regions. Intriguingly, the larger  $\delta^{18}\text{O}$  amplitude observed in the Tianmen record compared with the Pumu record may reflect additional mechanisms involving differences in moisture source and seasonal ground thaw dynamics between the monsoon and transition domains. Pumu Cave speleothem growth is restricted to warm and wet interglacial periods, with hiatuses persisting through cold and dry glacial intervals, depending largely on the effective ISM intensity. In contrast, speleothem growth in the transition domain of the TP reflects a combined influence of the AW and ISM circulation. Notably, the PM-1 stalagmite shows a hiatus corresponding to MIS9a despite the high NHSI condition, implying that a brief climatic amelioration with limited ISM precipitation may not be sufficient to promote the growth of speleothems in caves in the southern TP. This observation reinforces the hypothesis that interglacial temperature acts as a prerequisite for speleothem formation in the TP, while strong ISM precipitation, low ice volume and high CO<sub>2</sub> levels provide the sufficient conditions for the speleothem growth. In addition, the co-variation of Pumu  $\delta^{18}\text{O}$ ,  $\delta^{13}\text{C}$ , and trace element records further highlights the role of the ISM intensity in regulating local effective rainfall on orbital timescales. Moreover, environmental conditions in the region appear also to be influenced by global ice volume and/or atmospheric CO<sub>2</sub> levels, impacting soil and vegetation dynamics. These findings contribute to a more nuanced understanding of hydroclimate variability and the interplay between insolation, precipitation, and moisture sources in the TP.

## Authorship contribution statement

H. Wang and H. Cheng proposed and directed the study, and led the

writing. C. Pérez-Mejías, X. Wang and T. Li contributed to writing the original draft. H. Wang, and C. Yang collected the samples, and performed the stable isotope analysis. H. Li and S. Lei performed the trace element analysis. Y. Ning and R. L. Edwards contributed to  $^{230}\text{Th}$  dating. All authors discussed the results and contributed to improving the manuscript.

## Declaration of competing interest

The authors declare that they have no known competing financial interests or personal relationships that could have appeared to influence the work reported in this paper.

## Acknowledgments

This work was supported by the National Nature Science Foundation of China (NSFC) (grant number 42488201); the State Key Laboratory of Loess Science (grant number SKLLQGZR2401) and the NSFC (grant number 42472244).

## Appendix A. Supplementary data

Supplementary data to this article can be found online at <https://doi.org/10.1016/j.quascirev.2025.109625>.

## Data availability

All data and/or code is contained within the submission.

## References

- Allan, M., Delière, A., Verheyden, S., et al., 2018. Evidence for solar influence in a Holocene speleothem record (Père Noël cave, SE Belgium). *Quat. Sci. Rev.* 192, 249–262. <https://doi.org/10.1016/j.quascirev.2018.05.039>.
- An, W., Hou, S., Zhang, Q., et al., 2017. Enhanced recent local moisture recycling on the northwestern Tibetan Plateau deduced from ice core deuterium excess records. *J. Geophys. Res. Atmos.* 122, 12541–12556. <https://doi.org/10.1002/2017JD027235>.
- An, W., Hou, S., Zhang, W., et al., 2016. Possible recent warming hiatus on the northwestern Tibetan Plateau derived from ice core records. *Sci. Rep.* 6, 32813. <https://doi.org/10.1038/srep32813>.
- An, Z., Colman, S., Zhou, W., et al., 2012. Interplay between the westerlies and Asian monsoon recorded in lake Qinghai sediments since 32 ka. *Sci. Rep.* 2, 619. <https://doi.org/10.1038/srep00619>.
- An, Z., Kutzbach, J.E., Prell, W.L., et al., 2001. Evolution of Asian monsoons and phased uplift of the Himalaya-Tibetan plateau since Late Miocene times. *Nature* 411, 62–66. <https://doi.org/10.1038/35075035>.
- Baker, A., Ito, E., Smart, P.L., et al., 1997. Elevated and variable values of  $^{13}\text{C}$  in speleothems in a British cave system. *Chem. Geol.* 136, 263–270. [https://doi.org/10.1016/S0009-2541\(96\)00129-5](https://doi.org/10.1016/S0009-2541(96)00129-5).
- Baldini, J.U.L., McDermott, F., Fairchild, I.J., 2006. Spatial variability in cave drip water hydrochemistry: implications for stalagmite paleoclimate records. *Chem. Geol.* 235, 390–404. <https://doi.org/10.1016/j.chemgeo.2006.08.005>.
- Batchelor, C.J., McGee, D., Shakun, J.D., et al., 2024. Insights into changing interglacial conditions in subarctic Canada from MIS 11 through MIS 5e from seasonally resolved speleothem records. *Geophys. Res. Lett.* 51, e2024GL108459. <https://doi.org/10.1029/2024GL108459>.
- Battisti, D.S., Ding, Q., Roe, G.H., 2014. Coherent pan-Asian climatic and isotopic response to orbital forcing of tropical insolation. *J. Geophys. Res. Atmos.* 119 (11). <https://doi.org/10.1002/2014JD021960>, 997–12,020.
- Bereiter, B., Eggleston, S., Schmitt, J., et al., 2015. Revision of the EPICA Dome C CO<sub>2</sub> record from 800 to 600 kyr before present. *Geophys. Res. Lett.* 42, 542–549. <https://doi.org/10.1002/2014GL061957>.
- Berger, A.L., 1978. Long-term variations of caloric insolation resulting from the Earth's orbital elements. *Quat. Res.* 9 (2), 139–167. [https://doi.org/10.1016/0033-5894\(78\)90064-9](https://doi.org/10.1016/0033-5894(78)90064-9).

- Bernal, J.P., Cruz, F.W., Strfkis, N.M., et al., 2016. High-resolution Holocene south American monsoon history recorded by a speleothem from Botuverá cave, Brazil. *Earth Planet Sci. Lett.* 450, 186–196. <https://doi.org/10.1016/j.epsl.2016.06.008>.
- Bhattacharya, A., Bolch, T., Mukherjee, K., et al., 2021. High Mountain Asian glacier response to climate revealed by multi-temporal satellite observations since the 1960s. *Nat. Commun.* 12, 4133. <https://doi.org/10.1038/s41467-021-24180-y>.
- Bolch, T., Kulkarni, A., Kääb, A., et al., 2012. The state and fate of Himalayan glaciers. *Science* 336 (6079), 310–314. <https://doi.org/10.1126/science.1215828>.
- Bosmans, J.H.C., Erb, M.P., Dolan, A.M., et al., 2018. Response of the Asian summer monsoons to idealized precession and obliquity forcing in a set of GCMs. *Quat. Sci. Rev.* 188, 121–135. <https://doi.org/10.1016/j.quascirev.2018.03.025>.
- Breitenbach, S.F.M., Lechleitner, F.A., Meyer, H., et al., 2015. Cave ventilation and rainfall signals in dripwater in a monsoonal setting—a monitoring study from NE India. *Chem. Geol.* 402, 111–124. <https://doi.org/10.1016/j.chemgeo.2015.03.011>.
- Bronk Ramsey, C., 2008. Deposition models for chronological records. *Quat. Sci. Rev.* 27 (1–2), 42–60. <https://doi.org/10.1016/j.quascirev.2007.01.019>.
- Cai, Y., Cheng, H., An, Z., et al., 2010. Large variations of oxygen isotopes in precipitation over south-central Tibet during Marine Isotope Stage 5. *Geology* 38 (3), 243–246. <https://doi.org/10.1130/G30306.1>.
- Cai, Y., Zhang, H., Cheng, H., et al., 2012. The Holocene Indian monsoon variability over the southern Tibetan Plateau and its teleconnections. *Earth Planet Sci. Lett.* 335–336, 135–144. <https://doi.org/10.1016/j.epsl.2012.04.035>.
- Cai, Z., Tian, L., Bowen, G.J., 2017. ENSO variability reflected in precipitation oxygen isotopes across the Asian Summer Monsoon region. *Earth Planet Sci. Lett.* 475, 25–33. <https://doi.org/10.1016/j.epsl.2017.06.035>.
- Chen, C., Huang, R., Yuan, D., et al., 2021b. Karst hydrological changes during the late-Holocene in Southwestern China. *Quat. Sci. Rev.* 258, 106865. <https://doi.org/10.1016/j.quascirev.2021.106865>.
- Chen, C., Li, T., 2018. Geochemical characteristics of cave drip water respond to ENSO based on a 6-year monitoring work in Yangkou Cave, Southwest China. *J. Hydrol.* 561, 896–907. <https://doi.org/10.1016/j.jhydrol.2018.04.061>.
- Chen, C., Yuan, D., Cheng, H., et al., 2021a. Human activity and climate change triggered the expansion of rocky desertification in the karst areas of Southwestern China. *Sci. China Earth Sci.* 64, 1761–1773. <https://doi.org/10.1007/s11430-020-9760-7>.
- Cheng, H., Edwards, R.L., Shen, C.-C., et al., 2013. Improvements in  $^{230}\text{Th}$  dating,  $^{230}\text{Th}$  and  $^{234}\text{U}$  half-life values, and U-Th isotopic measurements by multi-collector inductively coupled plasma mass spectrometry. *Earth Planet Sci. Lett.* 371–372, 82–91. <https://doi.org/10.1016/j.epsl.2013.04.006>.
- Cheng, H., Edwards, R.L., Wang, Y., et al., 2006. A penultimate glacial monsoon record from Hulu Cave and two-phase glacial terminations. *Geology* 34, 217–220. <https://doi.org/10.1130/G22289.1>.
- Cheng, H., Li, H., Sha, L., et al., 2022. Milankovitch theory and monsoon. *Innovation* 3 (6), 100338. <https://doi.org/10.1016/j.xinn.2022.100338>.
- Cheng, H., Spötl, C., Breitenbach, S., et al., 2016b. Climate variations of Central Asia on orbital to millennial timescales. *Sci. Rep.* 6, 36975. <https://doi.org/10.1038/srep36975>.
- Cheng, H., Zhang, H., Zhao, J., et al., 2019. Chinese stalagmite paleoclimate researches: a review and perspective. *Sci. China Earth Sci.* 62, 1489–1513. <https://doi.org/10.1007/s11430-019-9478-3>.
- Cheng, H., Zhang, P., Spötl, C., et al., 2012b. The climatic cyclicity in semiarid-arid central Asia over the past 500,000 years. *Geophys. Res. Lett.* 39, L01705. <https://doi.org/10.1029/2011GL050202>.
- Cheng, H., Edwards, R.L., Sinha, A., et al., 2016a. The Asian monsoon over the past 640,000 years and ice age terminations. *Nature* 534 (7609), 640–646. <https://doi.org/10.1038/nature18591>.
- Cheng, H., Sinha, A., Wang, X., et al., 2012a. The global paleomonsoon as seen through speleothem records from Asia and the Americas. *Clim. Dyn.* 39, 1045–1062. <https://doi.org/10.1007/s00382-012-1363-7>.
- Cheng, T., Chen, D., Wang, B., et al., 2024. Human-induced warming accelerates local evapotranspiration and precipitation recycling over the Tibetan Plateau. *Commun. Earth Environ.* 5, 388. <https://doi.org/10.1038/s43247-024-01563-9>.
- Clark, P.U., Shakun, D.J., Rosenthal, Y., et al., 2024. Global and regional temperature change over the past 4.5 million years. *Science* 383, 884–890. <https://doi.org/10.1126/science.adl1908>.
- Cruz, F.W., Burns, S.J., Jercinovic, M., et al., 2007. Evidence of rainfall variations in Southern Brazil from trace element ratios (Mg/Ca and Sr/Ca) in a late Pleistocene stalagmite. *Geochem. Cosmochim. Acta* 71, 2250–2263. <https://doi.org/10.1016/j.gca.2007.02.005>.
- Dansgaard, W., 1964. Stable isotopes in precipitation. *Tellus* 16, 436–468. <https://doi.org/10.3402/tellusa.v16.4893>.
- Dorale, J.A., Liu, Z., 2009. Limitations of Hendy test criteria in judging the paleoclimatic suitability of speleothems and the need for replication. *J. Cave Karst Stud.* 71, 73–80. <https://doi.org/10.1016/j.jas.2009.01.001>.
- Dykoski, C.A., Edwards, R.L., Cheng, H., et al., 2005. A high-resolution, absolute-dated Holocene and deglacial Asian monsoon record from Dongge Cave, China. *Earth Planet Sci. Lett.* 233 (1–2), 71–86. <https://doi.org/10.1016/j.epsl.2005.01.036>.
- Edwards, R.L., Chen, J.H., Wasserburg, G.J., 1987.  $^{238}\text{U}$ – $^{234}\text{U}$ – $^{230}\text{Th}$ – $^{232}\text{Th}$  systematic and the precise measurement of time over the past 500,000 years. *Earth Planet Sci. Lett.* 81, 175–192. [https://doi.org/10.1016/0012-821X\(87\)90154-3](https://doi.org/10.1016/0012-821X(87)90154-3).
- Fairchild, I.J., Borsato, A., Tooth, A.F., et al., 2000. Controls on trace element (Sr-Mg) compositions of carbonate cave waters: implications for speleothem climatic records. *Chem. Geol.* 166, 255–269. [https://doi.org/10.1016/S0009-2541\(99\)00216-8](https://doi.org/10.1016/S0009-2541(99)00216-8).
- Fairchild, I.J., Treble, P.C., 2009. Trace elements in speleothems as recorders of environmental change. *Quat. Sci. Rev.* 28, 449–468. <https://doi.org/10.1016/j.quascirev.2008.11.007>.
- Farinotti, D., Immerzeel, W.W., de Kok, R.J., et al., 2020. Manifestations and mechanisms of the Karakoram glacier anomaly. *Nat. Geosci.* 13, 8–16. <https://doi.org/10.1038/s41561-019-0513-5>.
- Fohlmeister, J., Voarintsoa, N.R.G., Lechleitner, F.A., et al., 2020. Main controls on the stable carbon isotope composition of speleothems. *Geochem. Cosmochim. Acta* 279, 67–87. <https://doi.org/10.1016/j.gca.2020.03.042>.
- Griffiths, M.L., Drysdale, R.N., Gagan, M.K., et al., 2010. Evidence for Holocene changes in Australian–Indonesian monsoon rainfall from stalagmite trace element and stable isotope ratios. *Earth Planet Sci. Lett.* 292, 27–38. <https://doi.org/10.1016/j.epsl.2010.01.002>.
- Han, J., Shao, Z., Cheng, H., et al., 2017. Climate change since 7ka BP revealed by a high-resolution stalagmite  $\delta^{18}\text{O}$  and  $\delta^{13}\text{C}$  record from Benle cave in Chamdo, Tibet. *Acta Geol. Sin.* 11, 2545–2556 (in Chinese).
- Hartmann, A., Eiche, E., Neumann, T., et al., 2013. Multi-proxy evidence for human-induced deforestation and cultivation from a late Holocene stalagmite from middle Java, Indonesia. *Chem. Geol.* 357, 8–17. <https://doi.org/10.1016/j.chemgeo.2013.08.026>.
- He, S., Richards, K., 2016. Stable isotopes in monsoon precipitation and water vapour in Naqu, Tibet, and their implications for monsoon moisture. *J. Hydrol.* 540, 615–622. <https://doi.org/10.1016/j.jhydrol.2016.06.046>.
- Hendy, C.H., Wilson, A.T., 1968. Palaeoclimatic data from speleothem. *Nature* 219, 48–51. <https://doi.org/10.1038/219048a0>.
- Hou, S., Zhang, W., Pang, H., et al., 2019. Apparent discrepancy of Tibetan ice core  $\delta^{18}\text{O}$  records may be attributed to misinterpretation of chronology. *Cryosphere* 13 (6), 1743–1752. <https://doi.org/10.5194/tc-13-1743-2019>.
- Hu, J., Emile-Geay, J., Tabor, C., et al., 2019. Deciphering oxygen isotope records from Chinese speleothems with an isotope-enabled climate model. *Paleoceanogr. Paleoclimatol.* 34, 2098–2112. <https://doi.org/10.1029/2019PA003741>.
- Huang, J., Zhou, X., Wu, G., et al., 2023. Global climate impacts of land-surface and atmospheric processes over the Tibetan Plateau. *Rev. Geophys.* 61, e2022RG000771. <https://doi.org/10.1029/2022RG000771>.
- Hugonnet, R., McNabb, R., Berthier, E., et al., 2021. Accelerated global glacier mass loss in the early twenty-first century. *Nature* 592, 726–731. <https://doi.org/10.1038/s41586-021-03436-z>.
- Immerzeel, W.W., Beek, L.P., Bierkens, M.F., 2010. Climate change will affect the Asian water towers. *Science* 328, 1382–1385. <https://doi.org/10.1126/science.1183188>.
- Immerzeel, W.W., Lutz, A.F., Andrade, M., et al., 2020. Importance and vulnerability of the world's water towers. *Nature* 577, 364–369. <https://doi.org/10.1038/s41586-019-1822-y>.
- Johnson, K.R., Hu, C., Belshaw, N.S., et al., 2006. Seasonal trace-element and stable-isotope variations in a Chinese speleothem: the potential for high-resolution paleomonsoon reconstruction. *Earth Planet Sci. Lett.* 244, 394–407. <https://doi.org/10.1016/j.epsl.2006.01.064>.
- Joswiak, D.R., Yao, T., Wu, G., et al., 2010. A 70-yr record of oxygen-18 variability in an ice core from the Tanggula Mountains, central Tibetan Plateau. *Clim. Past* 6 (2), 219–227. <https://doi.org/10.5194/cp-6-219-2010>.
- Jouzel, J., Masson-Delmotte, V., Cattani, O., et al., 2007. Orbital and millennial Antarctic climate variability over the past 800,000 Years. *Science* 317, 793–796. <https://doi.org/10.1126/science.1141038>.
- Kaspari, S., Mayewski, P., Kang, S., et al., 2007. Reduction in northward incursions of the South Asian monsoon since ~1400 AD inferred from a Mt. Everest ice core. *Geophys. Res. Lett.* 34, L16701. <https://doi.org/10.1029/2007GL030440>.
- Kaushal, N., Lechleitner, F.A., Wilhelm, M., et al., 2024. SISALv3: a global speleothem stable isotope and trace element database. *Earth Syst. Sci. Data* 16, 1933–1963. <https://doi.org/10.5194/essd-16-1933-2024>.
- Klose, J., Weber, M., Scholz, D., 2024. Central European warm phases recorded by episodic speleothem growth during MIS 3. *Commun. Earth Environ.* 5, 719. <https://doi.org/10.1038/s43247-024-01863-0>.
- Kraaijenbrink, P.D.A., Bierkens, M.F.P., Lutz, A.F., et al., 2017. Impact of a global temperature rise of 1.5 degrees Celsius on Asia's glaciers. *Nature* 549, 257–260. <https://doi.org/10.1038/nature23878>.
- Kutzbach, J.E., 1981. Monsoon climate of the early Holocene: climate experiment with the Earth's orbital parameters for 9000 years ago. *Science* 214, 59–61. <https://doi.org/10.1126/science.214.4516.59>.
- Lechleitner, F.A., Breitenbach, S.F.M., Cheng, H., et al., 2017. Climatic and in-cave influences on  $\delta^{18}\text{O}$  and  $\delta^{13}\text{C}$  in a stalagmite from northeastern India through the last deglaciation. *Quat. Res.* 88, 458–471. <https://doi.org/10.1017/qua.2017.72>.
- Lei, Y., Yang, K., Wang, B., et al., 2014. Response of inland lake dynamics over the Tibetan Plateau to climate change. *Clim. Change* 125, 281–290. <https://doi.org/10.1007/s10584-014-1175-3>.
- Li, H., Cheng, H., Wang, J., et al., 2018. Applications of Laser Induced Breakdown Spectroscopy to paleoclimate research: reconstructing speleothem trace element records. *Quat. Sci.* 38 (6), 1549–1551. <https://doi.org/10.11928/j.issn.1001-7410.2018.06.21> (in Chinese).
- Li, R., Cai, Z., Wang, C., et al., 2025. Multiple climate forcings decomposed from a Tibetan plateau ice core isotope record. *J. Geophys. Res. Atmos.* 130, e2024JD042929. <https://doi.org/10.1029/2024JD042929>.
- Li, T., Baker, J.L., Wang, T., et al., 2021. Early Holocene permafrost retreat in West Siberia amplified by reorganization of westerly wind systems. *Commun. Earth Environ.* 2, 199. <https://doi.org/10.1038/s43247-021-00238-z>.
- Li, T., Huang, C., Tian, L., et al., 2018. Variation of  $\delta^{13}\text{C}$  in plant-soil-cave systems in karst regions with different degrees of rocky desertification in southwest China. *J. Cave Karst Stud.* 80, 212–228. <https://doi.org/10.4311/2018ES0107>.
- Li, Y.W., Pérez-Mejías, C., Zhao, J., et al., 2022. Indian summer monsoon variations during the Younger Dryas as revealed by a laminated stalagmite record from the

- Tibetan Plateau. Quat. Sci. Rev. 278, 107375. <https://doi.org/10.1016/j.quascirev.2022.107375>.
- Li, Y., Su, F., Tang, Q., et al., 2022. Contributions of moisture sources to precipitation in the major drainage basins in the Tibetan Plateau. Sci. China Earth Sci. 65, 1088–1103. <https://doi.org/10.1007/s11430-021-9890-6>.
- Liang, Q., Sha, L., Li, J., et al., 2024. Seasonal variations and controls on triple oxygen and hydrogen isotopes in precipitation—a case study from monitoring in Southwest China. J. Geophys. Res. Atmos. 129, e2023JD040654. <https://doi.org/10.1029/2023JD040654>.
- Lisiecki, L.E., Raymo, M.E., 2005. A pliocene-pleistocene stack of 57 globally distributed benthic  $\delta^{18}\text{O}$  records. Paleoceanogr. Paleoclimatol. 20, 1–17. <https://doi.org/10.1029/2004PA001071>.
- Liu, X., Chen, B., 2000. Climatic warming in the Tibetan Plateau during recent decades. Int. J. Climatol. 20, 1729–1742. [https://doi.org/10.1002/1097-0088\(20001130\)20:14<1729::AID-JOC556>3.0.CO;2-Y](https://doi.org/10.1002/1097-0088(20001130)20:14<1729::AID-JOC556>3.0.CO;2-Y).
- Liu, X., Liu, J., Shen, C.-C., et al., 2020. Inconsistency between records of  $\delta^{18}\text{O}$  and trace element ratios from stalagmites: evidence for increasing mid-late Holocene moisture in arid central Asia. Holocene 30 (3), 369–379. <https://doi.org/10.1177/0959683619887431>.
- Liu, Y., Chen, H., Li, H., et al., 2021. What induces the interdecadal shift of the dipole patterns of summer precipitation trends over the Tibetan Plateau? Int. J. Climatol. 41, 5159–5177. <https://doi.org/10.1002/joc.7122>.
- Lyu, Y., Luo, W., Wang, Y., et al., 2023. Response of drip water Mg/Ca and Sr/Ca variations in ventilated caves to hydroclimate. Sci. Total Environ. 874, 162626. <https://doi.org/10.1016/j.scitotenv.2023.162626>.
- Man, W., Zhou, T., Jiang, J., et al., 2022. Moisture sources and climatic controls of precipitation stable isotopes over the Tibetan Plateau in water-tagging simulations. J. Geophys. Res. Atmos. 127, e2021JD036321. <https://doi.org/10.1029/2021JD036321>.
- Meyer, M.C., Aldenderfer, M.S., Wang, Z., et al., 2017. Permanent human occupation of the central Tibetan Plateau in the early Holocene. Science 355, 64–67. <https://doi.org/10.1126/science.aag0357>.
- Miles, E., McCarthy, M., Dehecq, A., et al., 2021. Health and sustainability of glaciers in high mountain Asia. Nat. Commun. 12, 2868. <https://doi.org/10.1038/s41467-021-23073-4>.
- Musgrove, M., Banner, J.L., 2004. Controls on the spatial and temporal variability of vadose dripwater geochemistry: Edwards aquifer, central Texas. Geochim. Cosmochim. Acta 68, 1007–1020. <https://doi.org/10.1016/j.gca.2003.08.014>.
- O’Neil, J.R., Clayton, R.N., Mayeda, T.K., 1969. Oxygen isotope fractionation in divalent metal carbonates. J. Chem. Phys. 51, 5547–5558. <https://doi.org/10.1063/1.1671982>.
- Olson, E., Gillikin, D.P., Piccirillo, L., et al., 2024. Cave monitoring in the Peruvian Andes reveals monsoon climate preserved in speleothem calcite. Chem. Geol. 667, 122315. <https://doi.org/10.1016/j.chemgeo.2024.122315>.
- Oster, J.L., Covey, A.K., Lawrence, C.R., et al., 2021. A reactive transport approach to modeling cave seepage water chemistry II: elemental signatures. Geochim. Cosmochim. Acta 311, 353–373. <https://doi.org/10.1016/j.gca.2021.06.040>.
- Owen, R.A., Day, C.C., Hu, C., et al., 2016. Calcium isotopes in caves as a proxy for aridity: modern calibration and application to the 8.2 kyr event. Earth Planet Sci. Lett. 443, 129–138. <https://doi.org/10.1016/j.epsl.2016.03.027>.
- Pang, H., Hou, S., Kaspari, S., et al., 2014. Influence of regional precipitation patterns on stable isotopes in ice cores from the central Himalayas. Cryosphere 8 (1), 289–301. <https://doi.org/10.5194/tc-8-289-2014>.
- Pang, H., Hou, S., Zhang, W., et al., 2020. Temperature trends in the northwestern Tibetan Plateau constrained by ice core water isotopes over the past 7,000 years. J. Geophys. Res. Atmos. 125, e2020JD032560. <https://doi.org/10.1029/2020JD032560>.
- Parrenin, F., Barnola, J.M., Beer, J., et al., 2007. The EDC3 chronology for the EPICA Dome C ice core. Clim. Past 3, 485–497. <https://doi.org/10.5194/cp-3-485-2007>.
- Pausata, F.S.R., Battisti, D.S., Nisancioglu, K.H., et al., 2011. Chinese stalagmite  $\delta^{18}\text{O}$  controlled by changes in the Indian monsoon during a simulated Heinrich event. Nat. Geosci. 4, 474–480. <https://doi.org/10.1038/ngeo1169>.
- Pavoni, M., Boaga, J., Carrera, A., et al., 2023. Brief communication: mountain permafrost acts as an aquitard during an infiltration experiment monitored with electrical resistivity tomography time-lapse measurements. Cryosphere 17, 1601–1607. <https://doi.org/10.5194/tc-17-1601-2023>.
- Pérez-Mejías, C., Moreno, A., Bernal-Wormull, J., et al., 2021. Oldest dryas hydroclimate reorganization in the eastern Iberian Peninsula after the iceberg discharges of Heinrich event 1. Quat. Res. 101, 67–83. <https://doi.org/10.1017/qua.2020.112>.
- Pérez-Mejías, C., Moreno, A., Sancho, C., et al., 2019. Orbital-to-millennial scale climate variability during marine isotope stages 5 to 3 in northeast Iberia. Quat. Sci. Rev. 224, 105946. <https://doi.org/10.1016/j.quascirev.2019.105946>.
- Pérez-Mejías, C., Wang, J., Ning, Y., et al., 2025. Climate controls on speleothem initial  $^{234}\text{U}/^{238}\text{U}$  ratios in midlatitude settings over two glacial cycles. Geochim. Cosmochim. Acta. <https://doi.org/10.1016/j.gca.2024.11.016>.
- Qiu, J., 2008. China: the third pole. Nature 454, 393–396. <https://doi.org/10.1038/454393a>.
- Ramisch, A., Lockot, G., Haberzettl, T., et al., 2016. A persistent northern boundary of Indian summer monsoon precipitation over Central Asia during the Holocene. Sci. Rep. 6, 25791. <https://doi.org/10.1038/srep25791>.
- Shean, D.E., Bhushan, S., Montesano, P., et al., 2020. A systematic, regional assessment of High Mountain Asia glacier mass balance. Front. Earth Sci. 7, 363. <https://doi.org/10.3389/feart.2019.00363>.
- Su, Z., Xie, Y., Huang, J., et al., 2024. Impact of the Tibetan plateau on global high-frequency temperature variability. J. Clim. 37, 4347–4365. <https://doi.org/10.1175/JCLI-D-23-0271.1>.
- Spratt, R.M., Lisiecki, L.E., 2016. A Late Pleistocene sea level stack. Clim. Past 12, 1079–1092. <https://doi.org/10.5194/cp-12-1079-2016>.
- Springer, G.S., Rowe, H.D., Hardt, B., et al., 2008. Solar forcing of Holocene droughts in a stalagmite record from West Virginia in east-central North America. Geophys. Res. Lett. 35, L17703. <https://doi.org/10.1029/2008GL034971>.
- Stein, A.F., Draxler, R.R., Rolph, G.D., et al., 2015. NOAA’s HYSPLIT atmospheric transport and dispersion modeling system. Bull. Am. Meteorol. Soc. 96, 2059–2077. <https://doi.org/10.1175/BAMS-D-14-00110.1>.
- Tabor, C.R., Otto-Bliesner, B.L., Brady, E.C., et al., 2018. Interpreting precession-driven  $\delta^{18}\text{O}$  variability in the south Asia monsoon region. J. Geophys. Res. Atmos. 123 (11), 5927–5946. <https://doi.org/10.1029/2018JD028424>.
- Thompson, L.G., Mosley-Thompson, E., Davis, M.E., et al., 2003. Tropical glacier and ice core evidence of climate change on annual to millennial time scales. Clim. Change 59 (1–2), 137–155. <https://doi.org/10.1023/A:1024472313775>.
- Thompson, L.G., Yao, T., Davis, M.E., et al., 2018. Ice core records of climate variability on the Third Pole with emphasis on the Guliya ice cap, western Kunlun Mountains. Quat. Sci. Rev. 188, 1–14. <https://doi.org/10.1016/j.quascirev.2018.03.003>.
- Thompson, L.G., Yao, T., Davis, M.E., et al., 2024. Ice core evidence for an orbital-scale climate transition on the Northwest Tibetan Plateau. Quat. Sci. Rev. 324, 108443. <https://doi.org/10.1016/j.quascirev.2023.108443>.
- Thompson, L.G., Yao, T., Davis, M.E., et al., 1997. Tropical climate instability: the last glacial cycle from a Qinghai-Tibetan ice core. Science 276, 1821–1825. <https://doi.org/10.1126/science.276.5320.1821>.
- Thompson, L.G., Severinghaus, J.P., Yao, T., et al., 2022. Use of  $\delta^{18}\text{O}_{\text{atm}}$  in dating a Tibetan ice core record of Holocene/Late Glacial climate. Proc. Natl. Acad. Sci. USA. 119 (45), e2205545119. <https://doi.org/10.1073/pnas.2205545119>.
- Tian, L., Masson-Delmotte, V., Stiveenard, M., et al., 2001. Tibetan Plateau summer monsoon northward extent revealed by measurements of water stable isotopes. J. Geophys. Res. 106 (D22). <https://doi.org/10.1029/2001JD900186>, 28,081e28,088.
- Tian, L., Yao, T., Li, Z., et al., 2006. Recent rapid warming trend revealed from the isotopic record in Muztagata ice core, eastern Pamirs. J. Geophys. Res. Atmos. 111, D13103. <https://doi.org/10.1029/2005JD006249>.
- Tian, L., Yao, T., Schuster, P.F., et al., 2003. Oxygen-18 concentrations and ice cores on the Tibetan Plateau. J. Geophys. Res. 108, 4293. <https://doi.org/10.1029/2002JD002173>.
- Treble, P., Shelley, J., Chappell, J., 2003. Comparison of high resolution sub-annual records of trace elements in a modern (1911–1992) speleothem with instrumental climate data from southwest Australia. Earth Planet Sci. Lett. 216, 141–153. [https://doi.org/10.1016/S0012-821X\(03\)00504-1](https://doi.org/10.1016/S0012-821X(03)00504-1).
- Tremaine, D.M., Froehlich, P.N., 2013. Speleothem trace element signatures: a hydrologic geochemical study of modern cave dripwaters and farmed calcite. Geochim. Cosmochim. Acta 121, 522–545. <https://doi.org/10.1016/j.gca.2013.07.026>.
- Vansteenberge, S., de Winter, N.J., Sinnesael, M., et al., 2020. Reconstructing seasonality through stable-isotope and trace-element analyses of the Proserpine stalagmite, Han-sur-Lesse cave, Belgium: indications for climate-driven changes during the last 400 years. Clim. Past 16, 141–160. <https://doi.org/10.5194/cp-16-141-2020>.
- Verheyden, S., Keppens, E., Fairchild, I., et al., 2000. Mg, Sr and Sr isotope geochemistry of a Belgian Holocene speleothem: implications for paleoclimate reconstructions. Chem. Geol. 169 (1–2), 131–144. [https://doi.org/10.1016/S0009-2541\(00\)0299-0](https://doi.org/10.1016/S0009-2541(00)0299-0).
- Vuille, M., Werner, M., Bradley, R., et al., 2005. Stable isotope in precipitation in the Asian monsoon region. J. Geophys. Res. 110, D23108. <https://doi.org/10.1029/2005JD006022>.
- Wang, H., Wang, X., Pérez-Mejías, C., et al., 2022. Orbital-scale hydroclimate variations in the southern Tibetan Plateau over the past 414,000 years. Quat. Sci. Rev. 291, 107658. <https://doi.org/10.1016/j.quascirev.2022.107658>.
- Wang, N., Yao, T., Thompson, L.G., et al., 2006. Strong negative correlation between dust event frequency and air temperature over the northern Tibetan Plateau reflected by the Malan Ice-Core record. Ann. Glaciol. 43, 29–33. <https://doi.org/10.3189/172756406781812339>.
- Wang, Y., Cheng, H., Edwards, R.L., et al., 2008. Millennial-and orbital-scale changes in the East Asian monsoon over the past 224,000 years. Nature 451, 1090–1093. <https://doi.org/10.1038/nature06692>.
- Wang, Z., Meyer, M.C., Hoffmann, D.L., 2016. Sedimentology, petrography and early diagenesis of a travertine–colluvium succession from Chusang (southern Tibet). Sediment. Geol. 342, 218–236. <https://doi.org/10.1016/j.sedgeo.2016.07.002>.
- Wang, Z., Yin, J., Cheng, H., et al., 2022. Climatic controls on travertine deposition in southern Tibet during the late Quaternary. Palaeogeogr. Palaeoclimatol. Palaeoecol. 589, 110852. <https://doi.org/10.1016/j.palaeo.2022.110852>.
- Warken, S.F., Fohlmeister, J., Schröder-Ritzrau, A., et al., 2018. Reconstruction of late Holocene autumn/winter precipitation variability in SW Romania from a high-resolution speleothem trace element record. Earth Planet Sci. Lett. 499, 122–133. <https://doi.org/10.1016/j.epsl.2018.07.027>.
- Wei, F., 1994. Karst and karst water of Tibet. In: Xie, Y., Yang, M. (Eds.), Human Activity and Karst Environment. Beijing Science and Technology Press, Guiyang, pp. 211–218.
- Wong, C.I., Banner, J.L., Musgrove, M., 2011. Seasonal dripwater Mg/Ca and Sr/Ca variations driven by cave ventilation: implications for and modeling of speleothem paleoclimate records. Geochim. Cosmochim. Acta 75, 3514–3529. <https://doi.org/10.1016/j.gca.2011.03.025>.
- Wu, G., Liu, Y., He, B., et al., 2012. Thermal controls on the Asian summer monsoon. Sci. Rep. 2, 404. <https://doi.org/10.1038/srep00404>.
- Wu, Y., Li, T., Li, J., et al., 2023. Variations in Asian summer monsoon and hydroclimate during Heinrich stadials 4 revealed by stalagmite stable isotopes and trace elements. Quat. Sci. Rev. 299, 107869. <https://doi.org/10.1016/j.quascirev.2022.107869>.

- Xu, F., Zhang, G., Woolway, R.I., et al., 2024. Widespread societal and ecological impacts from projected Tibetan Plateau lake expansion. *Nat. Geosci.* 17, 516523. <https://doi.org/10.1038/s41561-024-01446-w>.
- Xue, Y., Zhang, J., Su, Z., et al., 2023. Quantifying source effects based on rainwater  $\delta^{18}\text{O}$  from 10-year monitoring records in Southwest China. *Appl. Geochem.*, 105706. <https://doi.org/10.1016/j.apgeochem.2023.105706>.
- Yan, X., Zhang, X., Liu, B., et al., 2025. Asynchronicity of deglacial permafrost thawing controlled by millennial-scale climate variability. *Nat. Commun.* 16, 290. <https://doi.org/10.1038/s41467-024-55184-z>.
- Yang, K., Wu, H., Qin, J., et al., 2014. Recent climate changes over the Tibetan Plateau and their impacts on energy and water cycle: a review. *Global Planet. Change* 112, 79–91. <https://doi.org/10.1016/j.gloplacha.2013.12.001>.
- Yao, T., Bolch, T., Chen, D., et al., 2022. The imbalance of the Asian water tower. *Nat. Rev. Earth Environ.* 3, 618–632. <https://doi.org/10.1038/s43017-022-00299-4>.
- Yao, T., Duan, K., Thompson, L.G., et al., 2007. Temperature variations over the past millennium on the Tibetan Plateau revealed by four ice cores. *Ann. Glaciol.* 46, 362–366. <https://doi.org/10.3189/172756407782871305>.
- Yao, T., Masson-Delmotte, V., Gao, J., et al., 2013. A review of climatic controls on  $\delta^{18}\text{O}$  in precipitation over the Tibetan Plateau: observations and simulations. *Rev. Geophys.* 51, 525–548. <https://doi.org/10.1002/rog.20023>.
- Yao, T., Thompson, L.G., Shi, Y., et al., 1997. Climate variation since the Last Interglacial recorded in the Guliya ice core. *Sci. China Earth Sci.* 40, 662–668. <https://doi.org/10.1007/BF02877697>.
- Yao, T., Thompson, L.G., Yang, W., et al., 2012. Different glacier status with atmospheric circulations in Tibetan Plateau and surroundings. *Nat. Clim. Change* 2, 663–667. <https://doi.org/10.1038/nclimate1580>.
- Yao, T., Xue, Y., Chen, D., et al., 2019. Recent Third Pole's rapid warming accompanies cryospheric melt and water cycle intensification and interactions between monsoon and environment: multidisciplinary approach with observations, modeling, and analysis. *Bull. Am. Meteorol. Soc.* 100 (3), 423–444. <https://doi.org/10.1175/bams-d-17-0057.1>.
- Yao, T., Zhou, H., Yang, X., 2009. Indian monsoon influences altitude effect of  $\delta^{18}\text{O}$  in precipitation/river water on the Tibetan Plateau. *Chin. Sci. Bull.* 54, 2724–2731. <https://doi.org/10.1007/s11434-009-0497-4>.
- Ye, D., Wu, G., 1998. The role of the heat source of the Tibetan Plateau in the general circulation. *Meteorol. Atmos. Phys.* 67, 181–198. <https://doi.org/10.1007/BF01277509>.
- Yu, W., Yao, T., Thompson, L.G., et al., 2021. Temperature signals of ice core and speleothem isotopic records from Asian monsoon region as indicated by precipitation  $\delta^{18}\text{O}$ . *Earth Planet. Sci. Lett.* 554, 116665. <https://doi.org/10.1016/j.epsl.2020.116665>.
- Yu, W., Yao, T., Tian, L., et al., 2008. Relationships between  $\delta^{18}\text{O}$  in precipitation and air temperature and moisture origin on a south-north transect of the Tibetan Plateau. *Atmos. Res.* 87, 158–169. <https://doi.org/10.1016/j.atmosres.2007.08.004>.
- Yuan, D., Cheng, H., Edwards, R.L., et al., 2004. Timing, duration, and transitions of the last interglacial Asian monsoon. *Science* 304, 575–578. <https://doi.org/10.1126/science.1091220>.
- Zentmyer, R., Myrow, P.M., Newell, D.L., 2008. Travertine deposits from along the south Tibetan fault system near Nyalam, Tibet. *Geol. Mag.* 145 (6), 753–765. <https://doi.org/10.1017/S0016756808005323>.
- Zhang, D., Qin, D., Hou, S., et al., 2005. Climatic significance of  $\delta^{18}\text{O}$  records from an 80.36 m ice core in the East Rongbuk glacier, mount Qomolangma (Everest). *Sci. China Earth Sci.* 48, 266–272. <https://doi.org/10.1360/02yd0219>.
- Zhang, G., Tao, T., Xie, H., et al., 2020. Response of Tibetan Plateau lakes to climate change: trends, patterns, and mechanisms. *Earth Sci. Rev.* 208, 103269. <https://doi.org/10.1016/j.earscirev.2020.103269>.
- Zhang, H., Griffiths, M.L., Chiang, J.C.H., et al., 2018. East Asian hydroclimate modulated by the position of the westerlies during Termination I. *Science* 362, 580–583. <https://doi.org/10.1126/science.aat9393>.
- Zhang, H., Zhang, X., Cai, Y., et al., 2021. A data-model comparison pinpoints Holocene spatiotemporal pattern of East Asian summer monsoon. *Quat. Sci. Rev.* 261, 106911. <https://doi.org/10.1016/j.quascirev.2021.106911>.
- Zhang, J., Li, T., 2019. Seasonal and interannual variations of hydrochemical characteristics and stable isotopic compositions of drip waters in Furong Cave, southwest China based on 12 years' monitoring. *J. Hydrol.* 572, 40–50. <https://doi.org/10.1016/j.jhydrol.2019.02.052>.
- Zhao, J., Cheng, H., Cao, J., et al., 2023. Orchestrated decline of Asian summer monsoon and Atlantic meridional overturning circulation in global warming period. *Innov. Geosci.* 1 (1). <https://doi.org/10.59717/j.xinn-geo.2023.100011>.